Relevance of Ge incorporation to control the physical behaviour of point defects in kesterite

Thomas Ratz,[1,2] Ngoc Duy Nguyen,[1] Guy Brammertz,[3] Bart Vermang,[2,3,4] and Jean-Yves Raty[1]

[1]*CESAM — Q-MAT — Solid State Physics, Interfaces and Nanostructures,*
Physics Institute B5a, Allée du Six Août 19, B-4000 Liège, Belgium
[2]*Institute for Material Research (IMO), Hasselt University,*
Agoralaan gebouw H, B-3590 Diepenbeek, Belgium
[3]*IMEC division IMOMEC — partner in Solliance,*
Wetenschapspark 1, B-3590 Diepenbeek, Belgium
[4]*Energyville, Thor Park 8320, B-3600 Genk, Belgium*

Supplementary Information

Theoretical framework

Defect formation energy $\Delta H_F(\alpha, q)$

Beyond materials properties predictions, the first-principles approach is a powerful tool to understand the behaviour of defects in semiconductor compounds [S1–S4]. Within the density functional theory (DFT) formalism, several assumptions are made to model lattice defects in order to balance the results accuracy and the required numerical and time cost. In this work, the supercell approach is considered and the calculations are performed with a 64-atoms supercell corresponding to an expansion of $2 \times 2 \times 2$ of the kesterite conventional cell as presented in **Figure S1**. The size of the computational box is assumed to be large enough to allow for the full relaxation of the defect-induced elastic constraint over the supercell dimension. Consequently, we assume no mechanical stress due to interaction between defects and their periodic repetitions produced by the applied periodic boundary conditions. In addition, the long range Coulomb interaction between charged defects is accounted for via a correction term added to the defect formation energy relation as described later on.
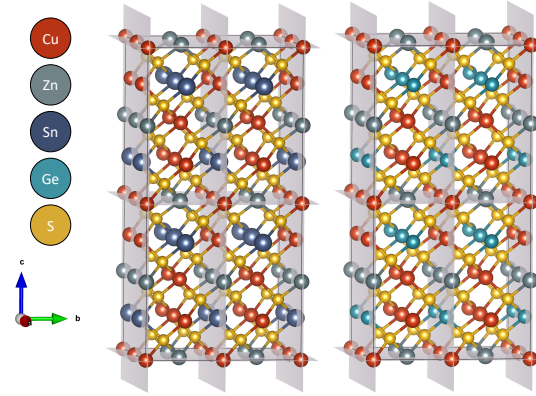

FIG. S1: Undefected kesterites 64-atoms supercells used to compute the defects formation energies. The supercell corresponds to an expansion of $2 \times 2 \times 2$ of the kesterite conventional cell as represented by the grey shadings.

Using the supercell approach, the formation energy of a defect α in a charge state q can be calculated as

$$\Delta H_F(\alpha, q, E_F, \mu_i) = E(\alpha, q) - E_{\text{host}} - \sum_i n_i (E_i + \mu_i) + q[\epsilon_{\text{VBM,host}} + E_F], \tag{S1}$$

where $E(\alpha, q)$ is the total energy of the supercell with a defect α in the charge state q. E_{host} is the total energy of the 64-atom undefected supercell while n_i is the number of atom(s) of the species i removed (< 0) from or added (> 0) to the host supercell with E_i, the energy per atom of the pure phase of the species i and μ_i, the chemical potential of the corresponding element. The third term accounts for an exchange of particles between the system under study and an external reservoir implying an energy transfer according to the chemical potential of the species. Then, assuming a defect in a charge state q, an extra term is added to this equation which considers an exchange of charge(s) between an external electronic reservoir and the system under study. In this term, $\epsilon_{\text{VBM,host}}$ refers to the valence band maximum (VBM) of the host supercell and E_F is the Fermi level acting as a parameter of the defect formation energy function and ranging from the VBM to the band gap energy E_G of the kesterite material. By taking a closer look into this equation, one can observed that for each intrinsic point defect α in a charge state q, the formation energy depends on two variables:

1. The energy exchanged due to the exchange of particles between an external reservoir and the system μ_i: this chemical potential parameter is linked to the experimental conditions under which the material is synthesised such as the atmosphere, the pressure, the temperature, ... *etc.* The values of μ_i are set by the position in the phase diagram of the material.

2. For a charged defect, the energy exchanged due to the transfer of charges related to the Fermi energy value $E_F \in [0; E_G]$.

Figure S2 shows a schematic representation of a defect formation energy considering three charge states: 0, -1, -2 is presented. Each charge state corresponds, according to Equation S1, to a line with a slope given by the charge state q. The lowest formation energy (the plain line) represents the minimal defect formation energy as a function of the Fermi level.

Furthermore, based on the formation energy of a given defect, it is possible to extract its ionisation levels. This allows to classify the behaviour of the defect via the determination of the energetic position of the ionisation levels. For a level located close to the edges of the band gap (i.e. the conduction band minimum: $E_F \simeq E_G$ or the valence band maximum: $E_F \simeq 0$), the defect can be classified as donor/acceptor. In opposition, defects close to the middle of the band gap will be classified as deep defects or recombination centres which could lead to a degradation of the solar cell performances depending on the defect concentration and carrier capture cross section. The defect ionisation energies are calculated using the following relation:

$$\mathcal{E}(\alpha, q, q') = \frac{\Delta H_F(\alpha, q) - \Delta H_F(\alpha, q')}{q' - q}, \tag{S2}$$

where q and q' are the charge states of the defect α considered for the transition. As a consequence, this transition energy correspond to the Fermi energy E_F for which the defect in a charge state q has the same formation energy as the defect in a charge state q'. Furthermore, as shown in Figure S2, the transition levels correspond to the intersection between each dashed line. These transitions are represented via a marker whose abscissa corresponds to the energetic position of the transition level in the materials band gap.
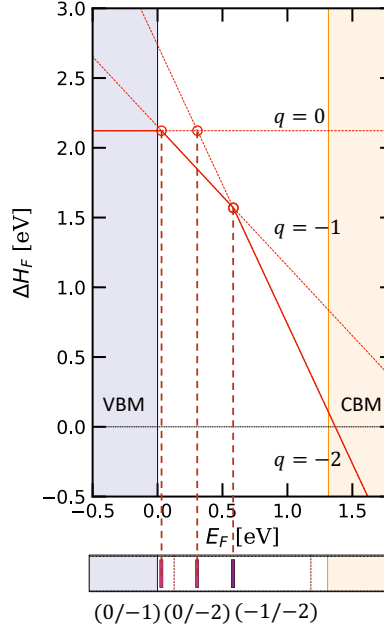

FIG. S2: Schematic representation of the evolution of a defect formation energy in which three charge states are considered: 0, -1, -2 giving three possible transition levels: (0/-1), (0/-2) and (-1/-2). The different charge state lines are represented using a dashed style.

Then, to compute the Fermi energy level E_F under thermodynamic equilibrium conditions as described in solid state physics, one can used the charge neutrality equation [S1]:

$$\sum_{\alpha, q} qC(\alpha(q)) + p - n = 0, \tag{S3}$$

where n, p is respectively the electron and the hole concentrations, and $C(\alpha(q))$ is the concentration of the defect α in its charge state q. The defect concentration $C(\alpha(q))$ is directly related to its formation energy as follow:

$$C(\alpha(q)) = N \exp\left(\frac{-\Delta H_F(\alpha, q)}{k_B T}\right), \tag{S4}$$

with N the number of possible sites where the defect α could be formed. In addition, the integration of the electronic density of states g(E) multiplied by the Dirac distribution gives the number of charge carrier participating to the materials conductivity (n- or p-type). Therefore, one can write:

$$n - p = \int_{-\infty}^{\infty} dE \frac{g(E)}{1 + \exp(E - E_F/k_B T)} - N_e = \sum_{\alpha, q} qC(\alpha(q)), \tag{S5}$$

where N_e the number of electron in the neutral bulk cell. Moreover, for a non-degenerate semiconductor, the electron (resp. hole) concentration can be assumed to follow a Boltzmann distribution:

$$n = N_C \exp\left(-\frac{E_C - E_F}{k_B T}\right) \tag{S6}$$

$$p = N_V \exp\left(-\frac{E_F - E_V}{k_B T}\right), \tag{S7}$$

where $N_C = 2\left(\frac{2\pi m_e^* k_B T}{h^2}\right)^{3/2}$ and $N_V = 2\left(\frac{2\pi m_h^* k_B T}{h^2}\right)^{3/2}$. With h the planck constant.

Using the electron (resp. hole) effective masses m_e^* (resp. m_h^*) of Ref.[S5], the Fermi energy E_F can be iteratively found using Equation S5. In this work, the Fermi energy under thermodynamic equilibrium conditions was assumed to be found for a charge concentration criterion value upon 5×10^{13} cm^{-3}.
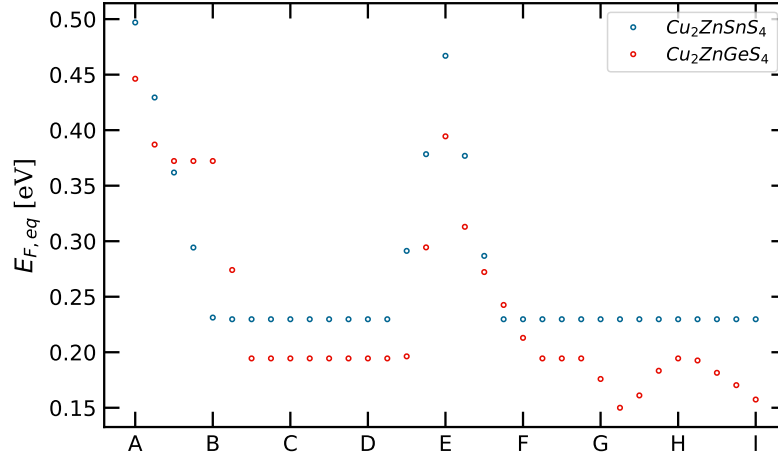

FIG. S3: Evolution of the Fermi energy level under thermodynamic equilibrium conditions as a function of the stoichiometry path as labelled in Figure 2 of the paper. See Table S2 for the specific chemical potential values.

Phase diagram

A variation in the material synthesis conditions can induce changes to the thin film composition and, consequently, the environment in which the defect will be formed. As a result, the formation energy of the point defect and its concentration will be impacted accordingly to the amount of energy required for the exchange of particles necessary

to form the defect. This energetic cost is described by the chemical potential of the chemical species (μ_i) which is defined as the Gibbs free energy variation caused by the exchange of particles between the system and an external reservoir, namely: $\mu_i = (\frac{dG}{dN_i})$ [S1]. One thus has to determine the chemical potentials μ_i that lead to the formation of a stable kesterite phase without any secondary phase. In order to address this challenge, kesterite phase diagrams have to be computed by fulfilling the following thermodynamic conditions :

(i) First, each chemical potential related to a species should favour the formation of the kesterite material instead of the species pure crystalline phase. A chemical potential value equal to 0 corresponding to the pure element crystalline phase (*e.g.* $\mu_{Cu} = 0$ implies a pure phase of Cu), the chemical potential values should be strictly negative to avoid the formation of pure compounds. This condition is expressed by the following inequalities:

$$\mu_{Cu} < 0, \mu_{Zn} < 0, \mu_X < 0, \mu_S < 0. \tag{S8}$$

(ii) Second, the sum of the chemical potentials must be equal to the formation energy of the desired compound, *i.e.* the kesterite material: Cu_2ZnXS_4 (X =Sn,Ge). This condition means that under thermodynamic equilibrium conditions, the desired stable phase is the kesterite compound:

$$\Delta H_F(Cu_2ZnXS_4) = 2\mu_{Cu} + \mu_{Zn} + \mu_X + 4\mu_S. \tag{S9}$$

Based on this equation and knowing the kesterite formation energy, one variable can be isolated as follow:

$$\mu_S = [\Delta H_F(CZXS) - \mu_{Zn} - \mu_X - 2\mu_{Cu}]/4. \tag{S10}$$

As a result, the phase diagram of this quaternary compound can be represented as a 3-dimensional map. For the sake of clarity, in this work, we represent the kesterite phase diagrams using a 2D-plot (μ_X (X=Sn,Ge) VS μ_{Zn}) for a fixed value of μ_{Cu}.

(iii) Third, based on the chemical species involved, several secondary phases could form. It is known that kesterite compounds are synthesised through a chemical path including binary or ternary compounds [S6]. Nevertheless, such secondary phases are detrimental for solar cell applications and are consequently undesired [S7]. The condition to be respected to avoid their formation can be expressed as follow: the sum of the involved chemical species potential values must be lower than the formation energy of the secondary phase under consideration. The formation energy of a compound being the difference between the compound total energy and the pure phase energy of each element within the compound: $\Delta H_F(A_iB_j) = E_{A_i,B_j} - n_iE_A - n_jE_B$.

$$\sum_i n_i\mu_i < \Delta H_F(X_i, n_i) \tag{S11}$$

Finally, in order to compute the formation energy of Ge-related defects (dopants) in the Sn-kesterite compound, one has to compute the Ge chemical potential μ_{Ge} within the Sn-matrix. To do so, additional secondary phases including the Ge element were calculated. Using Equation S9 combined with the criterion expressed in Equation S11, the Ge chemical potential was obtained.

As pointed out by Wexler *et.al.*in Ref.[S8], using the SCAN exchange-correlation functional, the formation energy in absolute value of every compound containing Ge is systematically underestimated with respect to experimental values. To deal with this effect, a correction of -0.27 eV/Ge was applied to each secondary phase formation energy for Ge-containing material.

From now on, using Equation S1 and the chemical potential values obtained from the description above, one can compute the defect formation energies for various charge states and thermodynamic environments.

Corrections terms

To accurately predict the defect formation energies, two correction terms were added to Equation S1. First, a potential alignment term, and second, a correction term dealing with the electrostatic interaction between charged defects located in the neighbour supercell images as a result of the periodic conditions used in the *ab initio* approach [S9, S10].

- The first correction arises from the divergence of the electrostatic potential upon charging. In consequence, the net energy is ill defined, and reference levels have to be aligned using Kohn-Sham energy levels of core orbitals of atoms located far from the defect.

- The second correction comes from the need to suppress the interaction between the charged defect located in the supercell and the ones located in the image supercells produced by the periodic boundary conditions applied. To do so, we correct the image charge interactions by adding to Equation S1, the following term :

$$\Delta E_i = [1 + c_{sh}(1 - \epsilon^{-1})]\frac{q^2 \alpha_M}{2\epsilon L},$$

(S12)

where c_{sh} is a value dependent on the crystal symmetry, ϵ is the dielectric constant, α_M is the crystal Madelung constant and L is the characteristic size of the supercell.

Methodology - Secondary phases

We computed the phase diagrams based on the thermodynamic conditions expressed previously. The pristine kesterite formation energies calculated are:

- $\Delta H_F(Cu_2ZnSnS_4) = -4.572$ eV

- $\Delta H_F(Cu_2ZnGeS_4) = -4.573$ eV

The following secondary phase formation energies were computed in both kesterites:

Cu$_2$ZnSnS$_4$ secondary phases	ΔH_F [eV]	Cu$_2$ZnGeS$_4$ secondary phases	ΔH_F [eV]
Cu_2SnS_3	-2.496	Cu_2GeS_3	-2.497
Cu_7S_4	-2.941	Cu_7S_4	-2.941
CuS	-0.493	CuS	-0.493
CuS_2	-0.215	CuS_2	-0.215
SnS	-0.847	GeS	-0.441
SnS_2	-1.237	GeS_2	-1.186
ZnS	-1.897	ZnS	-1.897
ZnS_2	-1.422	ZnS_2	-1.422
Cu_2GeS_3	-2.496	/	/
Cu_3Ge	-0.145	/	/
GeS	-0.441	/	/
GeS_2	-1.190	/	/
$SnGeS_3$	-2.065	/	/

TABLE S1: Secondary phases computed

In Table S2, we present the chemical potential values corresponding to the stoichiometry points labelled in the Figure 2 of the paper.

Chemical potentials	Cu$_2$ZnSnS$_4$					Cu$_2$ZnGeS$_4$			
	μ_{Cu} [eV]	μ_{Zn} [eV]	μ_{Sn} [eV]	μ_{S} [eV]	μ_{Ge} [eV]	μ_{Cu} [eV]	μ_{Zn} [eV]	μ_{Ge} [eV]	μ_{S} [eV]
A	-0.27	-1.25	-0.202	-0.64	-0.31	-0.27	-1.10	0	-0.73
B	-0.27	-1.52	-0.29	-0.55	-0.58	-0.27	-1.34	0	-0.67
C	-0.27	-1.82	-1.18	-0.26	-1.46	-0.27	-1.82	-1.17	-0.19
D	-0.27	-1.64	-1.36	-0.26	-1.46	-0.27	-1.64	-1.36	-0.19
E	-0.55	-1.56	-0.56	-0.34	-0.79	-0.55	-1.51	-0.40	-0.32
F	-0.55	-1.92	-0.92	-0.16	-1.21	-0.55	-1.87	-0.75	-0.14
G	-0.55	-2.08	-1.50	-0.05	-1.85	-0.55	-2.08	-1.49	-0.05
H	-0.55	-1.91	-1.68	-0.05	-1.85	-0.55	-1.90	-1.68	-0.05
I	-0.82	-2.00	-1.54	0	-1.87	-0.82	-1.97	-1.39	-0.02

TABLE S2: Chemical potential values corresponding to the labelled point in the phase diagrams (see Figure 2).

Kesterite crystal structure

In Table S3, we present the lattice structural parameters of both Cu$_2$ZnSnS$_4$ and Cu$_2$ZnGeS$_4$.

Parameters	Cu$_2$ZnSnS$_4$	Cu$_2$ZnGeS$_4$
a,b [Å]	5.40	5.30
c [Å]	10.79	10.51
V [Å^3]	314.9	294.87

TABLE S3: Kesterite lattice parameters.

[S1] C. Freysoldt *et al.*, *First-principles calculations for point defects in solids*, Reviews of modern physics **86**, 253 (2014).

[S2] S. Lany and A. Zunger, *Assessment of correction methods for the band-gap problem and for finite-size effects in supercell defect calculations: Case studies for ZnO and GaAs*, Physical Review B **78**, 235104 (2008).

[S3] C. Persson, Y.-J. Zhao, S. Lany, and A. Zunger, *n-type doping of CuInSe$_2$ and CuGaSe$_2$*, Physical Review B **72**, 035211 (2005).

[S4] J. S. Park, S. Kim, Z. Xie, and A. Walsh, *Point defect engineering in thin-film solar cells*, Nature Reviews Materials **3**, 194 (2018).

[S5] T. Ratz, J.-Y. Raty, G. Brammertz, B. Vermang, and N. D. Nguyen, *Opto-electronic properties and solar cell efficiency modelling of Cu$_2$ZnXS$_4$ (X= Sn,Ge,Si) kesterites*, Journal of Physics: Energy **3**, 035005 (2021).

[S6] S. Giraldo *et al.*, *Progress and perspectives of thin film kesterite photovoltaic technology: a critical Review*, Advanced Materials **31**, 1806692 (2019).

[S7] M. Dimitrievska, A. Fairbrother, E. Saucedo, A. Pérez-Rodríguez, and V. Izquierdo-Roca, *Secondary phase and Cu substitutional defect dynamics in kesterite solar cells: impact on optoelectronic properties*, Solar Energy Materials and Solar Cells **149**, 304 (2016).

[S8] R. B. Wexler, G. S. Gautam, and E. A. Carter, *Exchange-correlation functional challenges in modeling quaternary chalcogenides*, Physical Review B **102**, 054101 (2020).

[S9] S. L. Zunger and A, *Accurate prediction of defect properties in density functional supercell calculations*, p. 1 (2009).

[S10] C. Freysoldt, J. Neugebauer, and C. G. Van de Walle, *Fully ab initio finite-size corrections for charged-defect supercell calculations*, Physical review letters **102**, 016402 (2009).